Wireless Charging System for an Electric Autonomous Micro-transit Transportation Vehicle

Alireza Dayerizadeh, Andrew Galamb, Oscar Andres Montes, Srdjan Lukic
Department of Electrical and Computer Engineering
North Carolina State University
Raleigh, NC, USA
adayeri@ncsu.edu, aegalamb@ncsu.edu, omontes2@ncsu.edu, smlukic@ncsu.edu

***Abstract*—This paper details the design, testing and implementation of a wireless charging system for an autonomous micro-transit transportation (AMT) vehicle. Specifically, the paper covers the topology, controls, preliminary experimental results and integration approach within the Ecological personal transport (EcoPRT) autonomous vehicle. The SAE J2954 standard was used as a guideline for the systems overall mechanical and electrical design. The described system layout and methodology may be used in other autonomous charging applications in which power usage is high and frequent charging is required. Examples of this include autonomous vehicles used for both transportation and industrial applications. Experimental results of a scaled down lab set up are reported, detailing closed loop control of the constant current charging process and zero voltage switching behavior of the inverter output.**

***Index Terms*—Inductive Power Transfer, Wireless Charging, Wireless Power Transfer.**

I. Introduction

With the rise in adoption of electric and autonomous vehicles, wireless charging by means of inductive power transfer has seen a recent surge in interest [1]. In many of these applications, the efficiency from grid to vehicle is reaching levels above 90 percent [2] making wireless charging comparable to traditional plug-in forms of charging. In an ideal alignment scenario, efficiencies of up to 95 percent have been experimentally reported in high power tests [3]. Due to the convenience and efficiency of contactless operation, wireless charging is ideal for autonomous applications, allowing such equipped vehicles the ability to charge themselves, thereby increasing their autonomy [4].

Size, weight, and energy consumption are critical issues in most autonomous vehicle applications. In many cases, the high-power density of lithium ion batteries still falls short in allowing for long periods of sustained operation without the need for charging. In other cases, such as in drones, vehicle weight requirements further constrain energy storage capability [5]. Additionally, batteries are limited in the speed in which they may be charged, which limits the on-duty time of an autonomous vehicle. Autonomous charging aims to address these issues by allowing the vehicle to charge itself on a designated power transfer coil while on stand by or even continuously, such as in a dynamic application via a transmitting coil track [6], [7].

Fig. 1. $EcoPRT$ conceptual implementation (left) and prototype (right).

Wireless charging eliminates the need for moving heavy plugs and cables, and is inherently more reliable due to the lack of intermittent physical contacts [8]. In locations or conditions where an exposed physical contact is hazardous due to water, such as in outdoor applications or in an autonomous underwater vehicle, wireless charging provides a way to reach full autonomy for extended periods of time [9].

Furthermore, recent advances in wide-band gap devices, such as silicon carbide (SiC) and gallium nitride (GaN) are increasing the power density of power converters, allowing for more compact kW range wireless charging systems [10]. GaN devices in particular allow for high frequency operation within the industrial, scientific, medical (ISM) bands of 6.78 MHz and 13.56 MHz further increasing power density. For the purposes of this study and implementation, the operating frequency was set at 80 KHz in order to conform to the SAE J2954 standards [11].

This study focuses on a wireless charging system for the Ecological Personal Transport ($EcoPRT$) vehicle, which is an Autonomous Micro-Transit Transportation (AMT) vehicle that provides for a small autonomous and driverless vehicle network that operates on a fixed route system, as shown in Fig. 1. It should be noted that the focus of this paper is not the vehicle itself, but the wireless charging system for its batteries. Proof-of-concept testing and analysis of the closed-loop control and battery balancing system is performed on a low power scaled lab bench top set up. This set up represents the functionality of the final system and the results of this testing is reported in this study.

978-1-5386-9310-0/19/$31.00 ©2019 IEEE

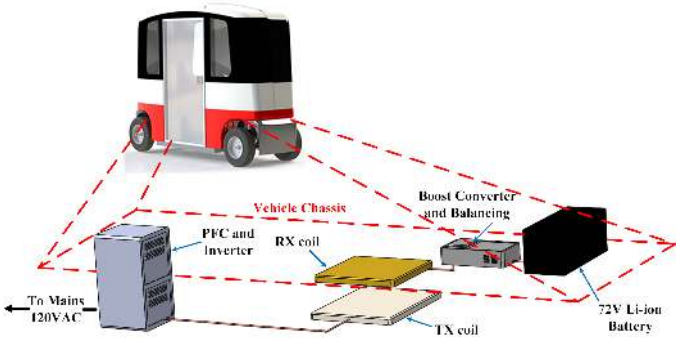

Fig. 2. . Integration of wireless charging system component enclosures within the vehicle chassis.

II. High Level System Overview

The envisioned system for the $EcoPRT$ vehicle is shown in Fig. 2 with system components housed in enclosures located both internal and external to the vehicle. The external housing contains the compensation capacitors, primary side digital signal processor (DSP), power factor correction (PFC) modules, gate driver board, inverter, and the necessary heat sinks with cooling fans. The UL rating of the PFC modules will allow the system to be directly connected to 120 V AC mains. The secondary side compensation capacitors, buck converter, DSP and battery balancing circuitry are housed in a 3D-printed enclosure within the vehicle and in close proximity to the vehicle battery. The final system proposed in this study will be designed to operate at Zone 1 charging level of 3.3 kW and a operating frequency of 80 KHz, keeping it within the bounds of the SAE J2954 Wireless Power Transfer for Light-Duty Plug-In/Electric Vehicles and Alignment Methodology standard [12]. The vehicle battery consists of two 36 V lithium ion battery packs in series. Lastly, as dictated by the previously mentioned SAE standard, a combined foreign object detection and live object protection system, detailed in a previous study [13], will be included. This system utilizes a thermal camera to detect any hazardous foreign metallic object or creature that would interfere with the system's safe operation.

III. Topology and Operation

The system topology is shown in Fig. 3. The LCL type compensation used on the primary side provides for constant current on the transmitting coil that is independent to changes in load, a well-known feature of this topology type [14], [15]. The secondary side buck converter modulates the real impedance R_{eq} by way of its duty cycle D with $R_L = V_{battery}/I_{battery}$ being considered representative of the impedance of the charging battery.

$$R_{eq} = \frac{\pi^2 R_L}{8D^2} \tag{1}$$

Utilizing a secondary series topology allows for only a real reflected impedance Z_r on the primary:

$$Z_r = \frac{\omega^2 M^2}{R_{eq}} \tag{2}$$

The mutual inductance is defined as M and $\omega = 2\pi f$. Based on Fig. 4, the impedance in the primary transmitting branch, Z_{tx}, at perfect coupling is:

$$Z_{tx} = j\omega L_1 + \frac{1}{j\omega C_{s1}} + Z_r \tag{3}$$

The total impedance seen by the receiver becomes:

$$Z_{in} = j\omega L_a + \frac{1}{j\omega C_1} || Z_{tx} \tag{4}$$

By Ohm's Law, the output current of the inverter I_{in}, assuming the fundamental component of the inverter's output voltage, is represented by:

$$I_{in} = \frac{2\sqrt{2}V_{DC}}{\pi(Z_{in})} \tag{5}$$

By current division, the transmitting coil track current, I_1, is:

$$I_1 = \frac{I_{in} Z_{tx}}{j\omega C} \tag{6}$$

Therefore, the total output power is represented by:

$$P_{out} = Re(Z_r) I_1^2 = \frac{\omega^2 M^2 I_1^2}{R_{eq}} \tag{7}$$

Maximum power output can be directly control via the inverter output current I_{in} by way of the inverter conduction angle [16]. However, for the purposes of this study, only secondary side control was used, with the duty cycle of the buck converter D controlling the current flow to the batteries under charge. This is performed using a PI controller that tracks and maintains the constant current to the battery under its varying state of charge. The PI controller's configuration is shown in Fig. 5. Also shown is the voltage PI controller, which maintains the constant voltage output across the batteries during the constant voltage state of charging. The output current of the buck converter and the voltage across each of the batteries is sensed to provide a reference for the controllers.

Due to the charging of multiple battery cells, a battery balancing method must be implemented to prevent overcharging of a cell, which can be hazardous. Numerous approaches for battery balancing exist. These include boost shunting, switched capacitor balancing and other approaches using power converters [17]. These approaches are utilized in any application where multiple cells are being charged, such as in an electric vehicle or microgrid [18], [19]. For the proposed system, a basic dissipative battery balancing system is implemented using relays and bleed resistors (Fig. 6). Each battery's voltage is tracked and maintained within a pre-determined tolerance to prevent overcharging. If either battery exceeds this voltage tolerance, a signal is sent to the appropriate relay allowing the battery to discharge into the bleed resister. This process is continuous throughout the battery's charging sequence.

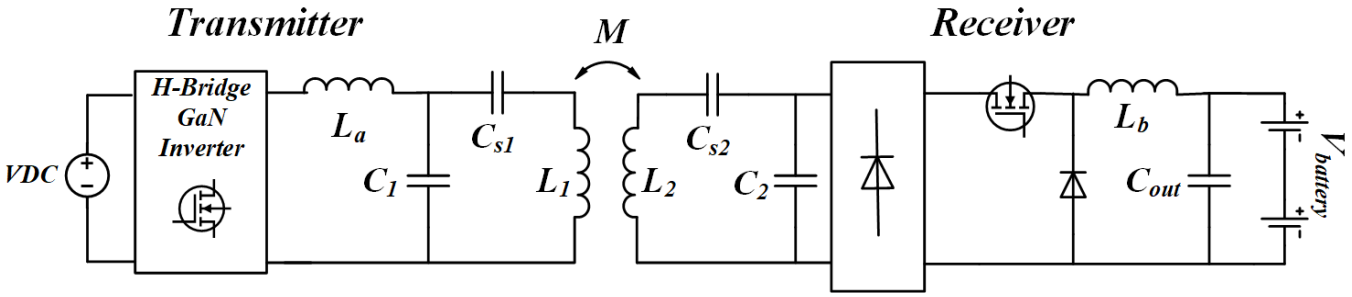

Fig. 3. System topology detailing the primary and secondary sections.

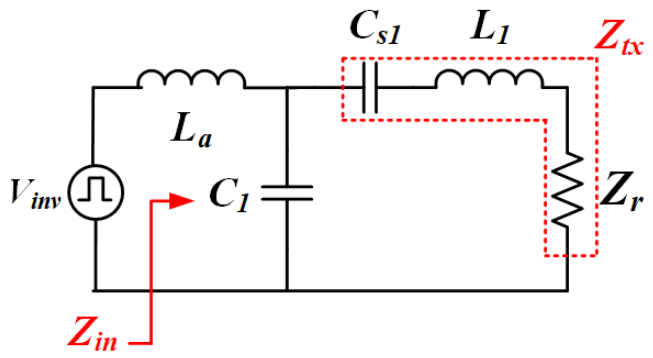

Fig. 4. Primary side with specified impedances shown.

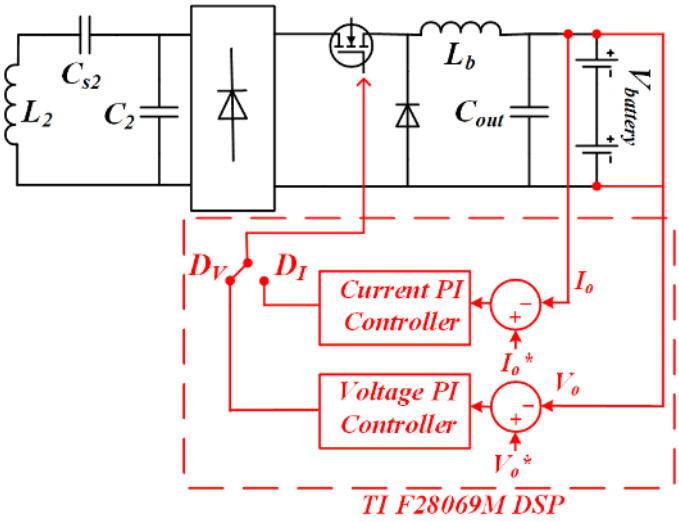

Fig. 5. Current and voltage PI controllers for closed loop control of battery state of charge during charging cycle.

IV. Experimental Results

A lab bench test bed of the proposed wireless charging system was built and tested. The complete system is shown in Fig. 8. The test bed system utilizes a Texas Instruments GaN inverter module board with LMG5200 half bridge GaN devices. The buck converter module on the secondary side is a Transphorm TDHBG2500P100 module equipped with two

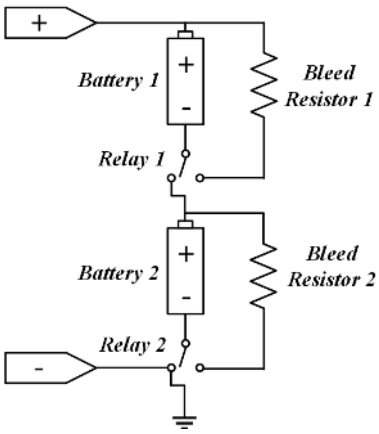

Fig. 6. Battery balancing circuit with bleed resistors.

TPH3212PS GaN FETs in synchronous configuration. Since the goal of this study is to demonstrate closed loop control and the battery balancing operation, this lower power set up, operating at approximately 20 W, was deemed sufficient. As previously stated, the implemented system will operate at 3.3 kW and utilize SiC MOSFETs and PFC modules in order to interface with an AC mains source. However, the GaN devices themselves are rated at 80 V and 10 A, making it possible to reliably implement them in 300 W to 600 W applications. This highlights a power dense solution to a wide variety of consumer and industrial electronics which operate within this power range.

The component values used for the bench top test are listed in Table I. Noting the high frequency and resonant operation of the system, the current ratings of the capacitors must be considered. For this reason, TDK C0G multilayer ceramic capacitors were used as compensation. The bridge inductor L_a was constructed using N87 core material. Both the primary and secondary side are interfaced with Texas Instruments F28069M Piccolo DSP boards for PWM generation, current/voltage monitoring and control. The final implementation of the system will utilize Bluetooth communication between these two DSPs which will allow for dual side control.

The coil design and assembly view are shown in Fig. 7. Specifications of the SAE J2954 were followed but scaled

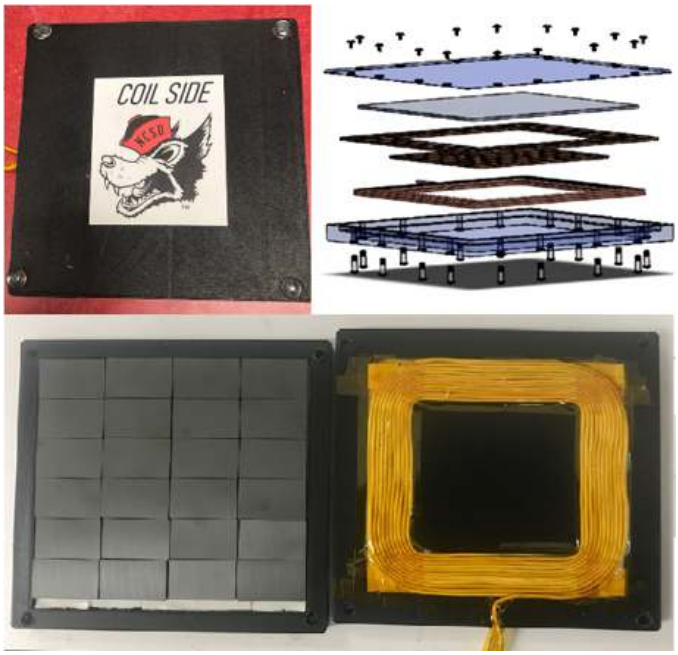

Fig. 7. Coil enclosure exterior (top left), Solidworks exploded view (top right), internal ferrite sheilding (bottom left) and coil with Kapton tape (bottom right).

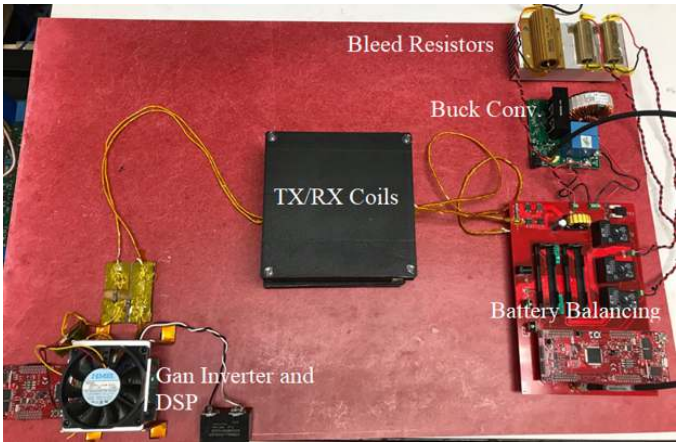

Fig. 8. Lab bench system test bed shown.

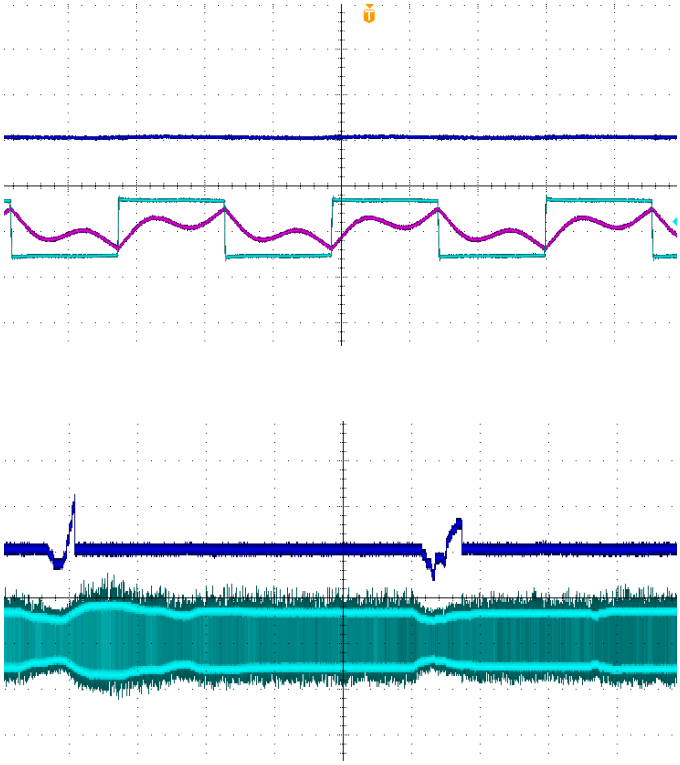

Fig. 9. Top: Inverter output current I_{in} (purple 10 A/div), output voltage (cyan 50 V/div) and current to load R_L (blue 250 mA/div). Bottom: Inverter output voltage (cyan 50 V/div) shown varying while current to the load R_L corrects and maintains 1 A (blue 250 mA/div).

TABLE I
SYSTEM COMPONENT VALUES

Segment	Component	Value
Transmitter	L_a	$4uH$
	L_1	$126uH$
	C_1	$200nF$
	C_{s1}	$33nF$
Receiver	L_2	$126uH$
	C_2	$33nF$
	R_{Load}	12.5Ω

down for use in this test. The coil assembly consisted of a 3D printed enclosure, 420 strand count litz wire, and 3F36 type ferrite tiles to channel the flux and improve coupling. The litz wire was wrapped in Kapton tape to provide isolation.

As can be observed in Fig. 9, zero voltage switching (ZVS) is obtained during operation, which improves the overall operational efficiency. The distorted current waveform is due to the presence of higher order harmonics due to the square wave voltage output of the inverter and the primary side LCL compensation. Detailed analysis of these harmonics is outside the scope of this paper, but has been reported in literature [20]. The overall DC source to load efficiency achieved was approximately 77 percent. Although this figure appears low, it must be noted that efficiency improves at higher power levels since a significant portion of losses remain constant. The implemented PI current controller can be seen tracking 1 A output under varying input voltage V_{DC} conditions demonstrating it's ability to maintain a constant current supply to the battery.

V. CONCLUSION

This paper details the implementation of a wireless charging system for an AMT vehicle. Detailed information is provided on the system topology, operation, and design. Hardware test results are provided to demonstrate power transfer and control capability. The approach developed in this study may apply to any autonomous vehicle type that requires frequent charging, such as drones and autonomous industrial equipment. Future work will including scaling the presented system and control methodology to the SAE J2954 Zone 1 charging level.

REFERENCES

[1] S. Lukic and Z. Pantic, "Cutting the cord: Static and dynamic inductive wireless charging of electric vehicles," *IEEE Electrification Magazine*, vol. 1, no. 1, pp. 57–64, Sep. 2013.

[2] S. Li and C. C. Mi, "Wireless power transfer for electric vehicle applications," *IEEE Journal of Emerging and Selected Topics in Power Electronics*, vol. 3, no. 1, pp. 4–17, March 2015.

[3] T. Nguyen, S. Li, W. Li, and C. C. Mi, "Feasibility study on bipolar pads for efficient wireless power chargers," in *2014 IEEE Applied Power Electronics Conference and Exposition - APEC 2014*, March 2014, pp. 1676–1682.

[4] M. Kesler, "Wireless charging of electric vehicles," in *2018 IEEE Wireless Power Transfer Conference (WPTC)*, June 2018, pp. 1–4.

[5] A. Raciti, S. A. Rizzo, and G. Susinni, "Drone charging stations over the buildings based on a wireless power transfer system," in *2018 IEEE/IAS 54th Industrial and Commercial Power Systems Technical Conference (I CPS)*, May 2018, pp. 1–6.

[6] A. Dayerizadeh and S. Lukic, "Saturable inductors for superior reflexive field containment in inductive power transfer systems," in *2018 IEEE Applied Power Electronics Conference and Exposition (APEC)*. IEEE, 2018, pp. 3183–3188.

[7] K. Lee, Z. Pantic, and S. M. Lukic, "Reflexive field containment in dynamic inductive power transfer systems," *IEEE Transactions on Power Electronics*, vol. 29, no. 9, pp. 4592–4602, Sep. 2014.

[8] J. M. Miller, O. C. Onar, and M. Chinthavali, "Primary-side power flow control of wireless power transfer for electric vehicle charging," *IEEE Journal of Emerging and Selected Topics in Power Electronics*, vol. 3, no. 1, pp. 147–162, March 2015.

[9] T. Kan, R. Mai, P. P. Mercier, and C. C. Mi, "Design and analysis of a three-phase wireless charging system for lightweight autonomous underwater vehicles," *IEEE Transactions on Power Electronics*, vol. 33, no. 8, pp. 6622–6632, Aug 2018.

[10] K. Rajashekara, "Present status and future trends in electric vehicle propulsion technologies," *IEEE Journal of Emerging and Selected Topics in Power Electronics*, vol. 1, no. 1, pp. 3–10, March 2013.

[11] *Wireless Power Transfer for Light Duty Plug-In Electric Vehicles and Alignment Methodology*, no. SAE Standard J2954, 2016.

[12] H. H. Wu, A. Gilchrist, K. Sealy, and D. Bronson, "A 90 percent efficient 5kw inductive charger for evs," in *2012 IEEE Energy Conversion Congress and Exposition (ECCE)*, Sep. 2012, pp. 275–282.

[13] T. Sonnenberg, A. Stevens, A. Dayerizadeh, and S. Lukic, "Combined foreign object detection and live object protection in wireless power transfer systems via real-time thermal camera analysis," in *2019 IEEE Applied Power Electronics Conference and Exposition (APEC)*. IEEE, 2019, pp. 1547–1552.

[14] H. H. Wu, A. Gilchrist, K. D. Sealy, and D. Bronson, "A high efficiency 5 kw inductive charger for evs using dual side control," *IEEE Transactions on Industrial Informatics*, vol. 8, no. 3, pp. 585–595, 2012.

[15] H. Feng, T. Cai, S. Duan, J. Zhao, X. Zhang, and C. Chen, "An lcc-compensated resonant converter optimized for robust reaction to large coupling variation in dynamic wireless power transfer," *IEEE Transactions on Industrial Electronics*, vol. 63, no. 10, pp. 6591–6601, Oct 2016.

[16] M. Borage, S. Tiwari, and S. Kotaiah, "Analysis and design of an lcl-t resonant converter as a constant-current power supply," *IEEE Transactions on Industrial Electronics*, vol. 52, no. 6, pp. 1547–1554, Dec 2005.

[17] J. Cao, N. Schofield, and A. Emadi, "Battery balancing methods: A comprehensive review," in *2008 IEEE Vehicle Power and Propulsion Conference*, Sep. 2008, pp. 1–6.

[18] N. Ghanbari, M. Mobarrez, and S. Bhattacharya, "A review and modeling of different droop control based methods for battery state of the charge balancing in dc microgrids," in *IECON 2018 - 44th Annual Conference of the IEEE Industrial Electronics Society*, Oct 2018, pp. 1625–1632.

[19] N. Ghanbari and S. Bhattacharya, "Soc balancing of different energy storage systems in dc microgrids using modified droop control," in *IECON 2018 - 44th Annual Conference of the IEEE Industrial Electronics Society*, Oct 2018, pp. 6094–6099.

[20] Z. Pantic, S. Bai, and S. M. Lukic, "Zcs *lcc*-compensated resonant inverter for inductive-power-transfer application," *IEEE Transactions on Industrial Electronics*, vol. 58, no. 8, pp. 3500–3510, 2011.